Materials Chemistry and Physics 112 (2008) 466–471

Contents lists available at ScienceDirect

Materials Chemistry and Physics

journal homepage: www.elsevier.com/locate/matchemphys

Atomic structure evolution of Zr–Ti and pure Zr during accumulated roll bonding by HA pair analysis

Y.C. Lo [a], J.C. Huang [a,*], S.P. Ju [b]

[a] Institute of Materials Science and Engineering, Center for Nanoscience and Nanotechnology, National Sun Yat-Sen University, Kaohsiung 804, Taiwan, ROC
[b] Department of Mechanical and Electro-Mechanical Engineering, National Sun Yat-Sen University, Kaohsiung 804, Taiwan, ROC

ARTICLE INFO

Article history:
Received 29 February 2008
Received in revised form 25 May 2008
Accepted 4 June 2008

Keywords:
Amorphous materials
Molecular dynamics
Phase transitions
Crystal structure

ABSTRACT

The gradual vitrification evolution of atom mixing and local atomic pairing structure of the binary Zr–Ti alloy and pure Zr during solid-state accumulative roll bonding (ARB) at room temperature is traced numerically by molecular dynamic simulation. It is found that icosahedra and more random clusters will gradually develop with increasing ARB cycles in the Zr–Ti alloy, forming amorphous atomic packing. Following the idea for Zr–Ti, the vitrification of pure Zr layers during ARB is simulated. The crystalline pure Zr can be vitrified in the simulation provided that the rolling speed is high enough and the rolling temperature is maintained at around 300 K.

1. Introduction

The two main paths for preparing the metallic amorphous materials are rapid cooling and solid-state reaction. Mechanical alloying (MA) [1–5] and accumulative roll bonding (ARB) [6–11] are considered to be feasible solid-state vitrification reaction methods for over a decade. Compared with the MA method which has been widely and systematically studied for numerous alloys, such as Co–Ti [12,13], Zr–Cu [5,14] and Zr–Ni [15,16] systems, the ARB-induced amorphization has received relatively less attention in terms of atomic structure evolution [17–20].

It has been shown lately [21–24] that local icosahedra packing can be formed during the course of rapid cooling. This is because that the short-range-ordered icosahedra clusters are easier to form as compared with the long-range-ordered structures. The binding energy of icosahedrons (in its absolute magnitude) is also slightly higher than the close-packed arrangement [21–24]. On the other hand, during the solid–state ARB process, the amorphous phase is obtained by the strain-induced diffusion of different metallic grains and the system does not contain any short-range ordering in the initial condition. According to our previous ARB experimental studies at ambient temperature [17–20] of binary Zr-based alloys made by ARB, the grain size of the ARB specimen was gradually refined down to ~2 nm, such nanocrystals would disappear in the matrix and form the complete amorphous phase upon subsequent ARB passes. The role played by the short-range ordering, such as icosahedra or other packing forms, during solid-state vitrification is still not well understood.

Molecular dynamics (MD) simulations have been successfully applied to analyze the structure, thermodynamic and dynamic properties of rapidly cooled alloys and the glass forming atomic mechanism [21–27]. Further, Honeycutt and Anderson [21] has used the pair analysis technique (termed as the HA pair index) to study the local structure features in disordered systems such as liquid and glass in early years. This approach provides clear information about the local symmetry of atomic arrangement more than the common pair correlation function, and has been used to simulate the grain boundary microstructure transition, local cluster structure, and glass forming of metallic alloys under the rapid cooling condition.

The first attempt to apply the HA index in the solid state vitrification such as ARB, which involves atomic diffusion and amorphization driven by the imposed shear rolling stress, was made recently on the Zr–Ni ARB system [20]. It has been known that the Zr–Ni alloy exhibits a high glass-forming ability (GFA) during rapid quenching, due to the large atomic radius difference (23%) and the large negative heat of mixing ($-49\,kJ\,mol^{-1}$) between Zr and Ni. In this study, the further extension of this method is made on the binary Zr–Ti and pure Zr multilayers during the repeated ARB strain-and-stack procedure. Zr and Ti are both of the hexagonal close-packed (HCP) structure. The heat of mixing between Zr and Ti is nearly zero. Meanwhile, the atomic radius (r) difference between Zr and Ti is only 8% (r_{Zr} = 0.160 nm and r_{Ti} = 0.148 nm). For the above characteristics, the Zr–Ti binary system can form an

* Corresponding author. Tel.: +886 7 5252000x4063; fax: +886 7 5254099.
E-mail address: jacobc@mail.nsysu.edu.tw (J.C. Huang).

0254-0584/$ – see front matter © 2008 Elsevier B.V. All rights reserved.
doi:10.1016/j.matchemphys.2008.06.001

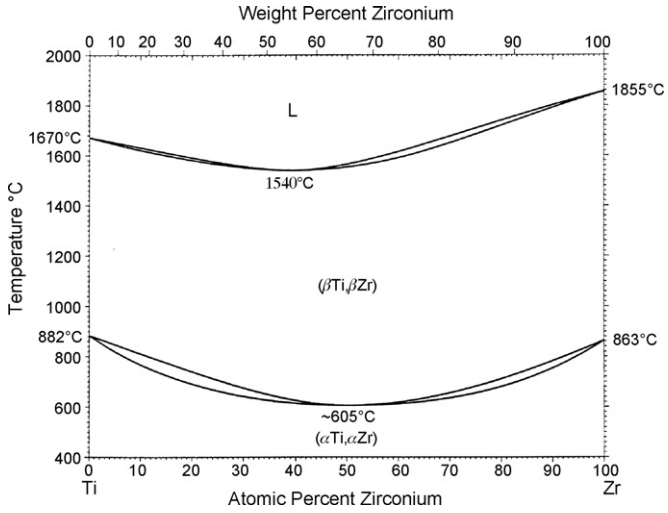

Fig. 1. Equilibrium phase diagrams for Zr–Ti [28].

isomorphous phase diagram without any intermetallic compound. The Zr–Ti equilibrium phase diagram [28] is shown in Fig. 1.

2. Simulation

The many-body tight binding potential is adopted to model the interatomic interactions of the binary Zr–Ti and pure Zr multilayers during the repeated ARB strain-and-stack procedure. Then, the gradual evolutions of atom mixing and local atomic crystal structure of the binary alloys are traced numerically by the radial distribution function (RDF) and the Honeycutt–Anderson (HA) pair analysis technique. Similar attempts focusing on the study of the amorphous phase growth in interface of bi-layers have been tried by Lund and Schuh [29] and Delogu and Cocco [30] in terms of RDF, hence it is concentrated in this report on the function of icosahedra and other intermetallic compound clusters on the microstructural transition during the ARB process.

In the current MD simulation model of the ARB process, a bi-layered structure consisting of HCP Zr coupled with the HCP Ti elemental layers, measuring 20 nm in width, 20 nm in length and 12 nm in thickness for each elemental layer, was set to be the starting alloy model in order to trace the final cyclic transformation stage between nanocrystalline and amorphous phases during ARB. The designed amounts in the Zr–Ti binary system are 116,064 Zr atoms and 118,184 Ti atoms. As for the pure Zr multilayer simulation, the number of atoms is 232,128. The Velocity Verlet algorithm [31] is employed to calculate the trajectories of the atoms and the scaling method is adopted during the simulation to control the system temperature at 300 K. The atomic interactions between different kinds of atom have all been included in simulation model. The atoms interact via many-body tight-binding potential is adopted to model all of the atomic interactions in the system [32–34]. The simulation of the ARB was done for two rolling speed, a higher one at 0.025 nm fs^{-1} and a lower one at 0.01 nm fs^{-1}.

3. Results and discussion

The transition from the nanocrystalline into amorphous phases at the final ARB stage is characterized in terms of the RDF and HA pair. In general, RDF is a statistical average for all configurations in the system; it is a powerful method to provide atomic pairs information but difficult to determine details of the local structural changes in the disorder system. The HA pair index can trace the local symmetry of atomic arrangement in liquid or glass. In the HA technique, two atoms are viewed as forming a bond pair if they are within a given cutoff distance that equals the first minimum in the partial radial distribution function (for example, Zr–Zr, Ti–Ti and Ti–Zr in the Zr–Ti system). There is a sequence of four integers to characterize the local structures according to the HA index. The first integer is the indication to characterize whether the atoms bonded in the HA pair are the near neighbors. The integer of "1" represents that the atoms are indeed near neighbors, and the integer of "2" means they are not. The second integer is the number of the near neighbors shared by the HA pair. The third integer denotes the number of bonds among the shared neighbors. When the first three indices are identical but the bond geometries are different, the forth integer is added.

According to this method, different HA indices will represent different local structures, as shown some examples in Fig. 2. For example, the 1421 and 1422 pairs will exist predominantly in the close-packed crystalline structure such as face-centered cubic (FCC) and HCP. In pure FCC crystals, the predominant pairs would be the 1421 ones; while in the pure HCP crystals, there are typically around 50% of the 1421 and 50% of the 1422 pairs. The 1551, 1541 and 1431 pairs are referred to the common short-range local structures of an amorphous or liquid state. The 1551 pair is particularly characteristic of the icosahedra ordering. The 1541 pair is the index for the icosahedra-defect local structure, and the 1431 one is the index for the FCC-defect structure. The 1441 and 1661 pairs are characteristics of the body-centered cubic (BCC) structure. Finally, the 1321 is a packing related to rhombohedra, and this pair tends to evolve when the icosahedra 1551 packing is formed and can be viewed as the side product accompanying the icosahedra atomic packing.

Since the heat of mixing between Zr and Ti is ~0 kJ mol^{-1}, the Zr–Ti system is generally considered to be a system that is difficult to form amorphous random atomic packing, provided that only

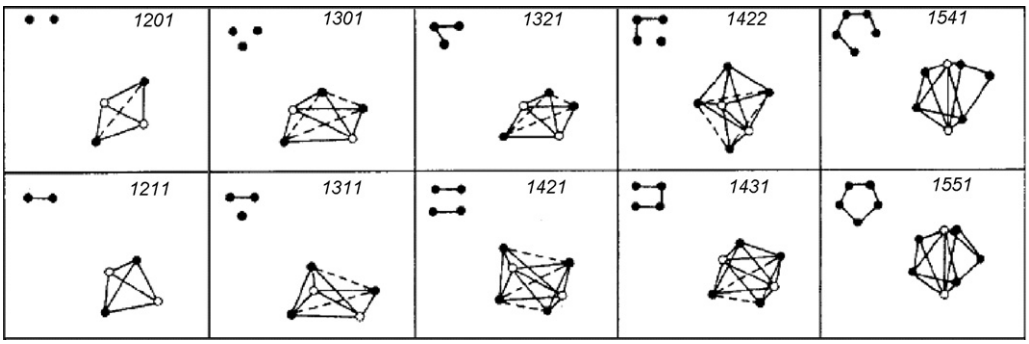

Fig. 2. The schematic drawing of the related HA pairs [21].

thermodynamic factors are under consideration. Instead, it has the tendency to form complete HCP solid solution. However, with the severe mutual deformation imposed by the shear force during ARB, this system has been demonstrated to form the amorphous packing after around 90 cycles of ARB [17–20].

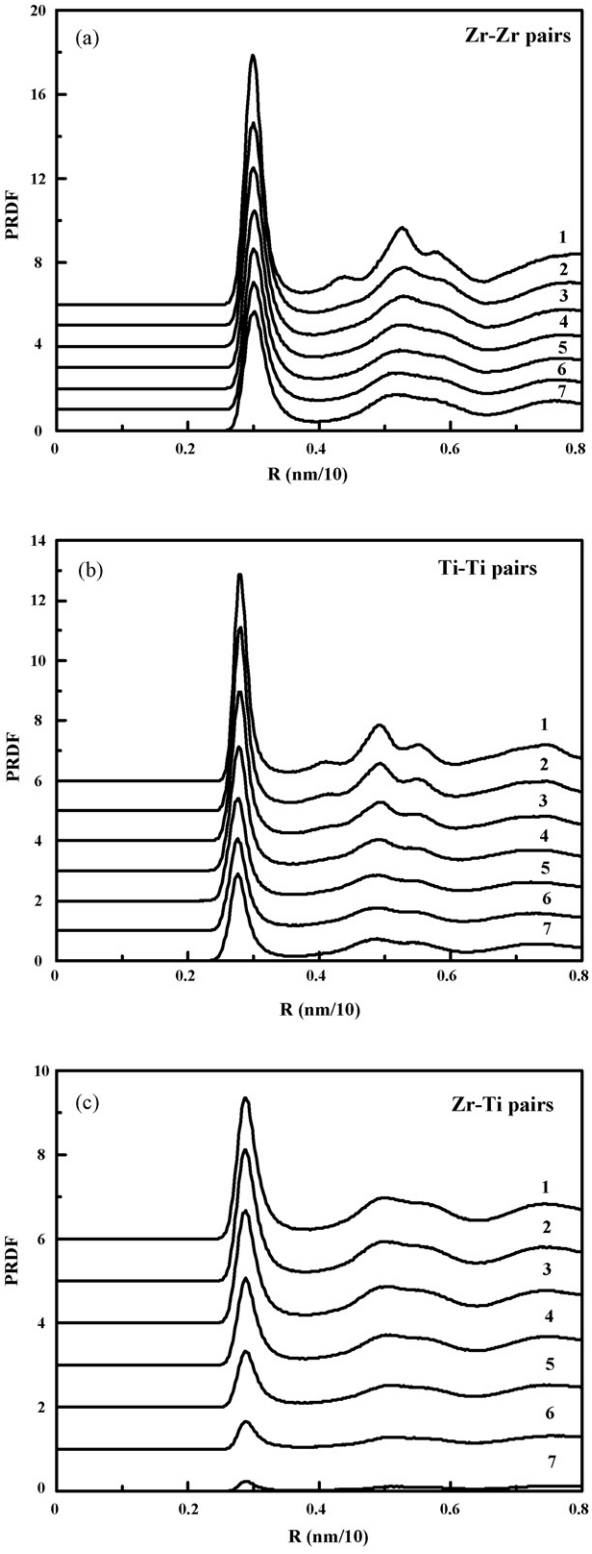

Fig. 3. PRDF of the Zr–Ti alloys during different ARB cycles: (a) Zr–Zr pair, (b) Ti–Ti pair, and (c) Zr–Ti pair.

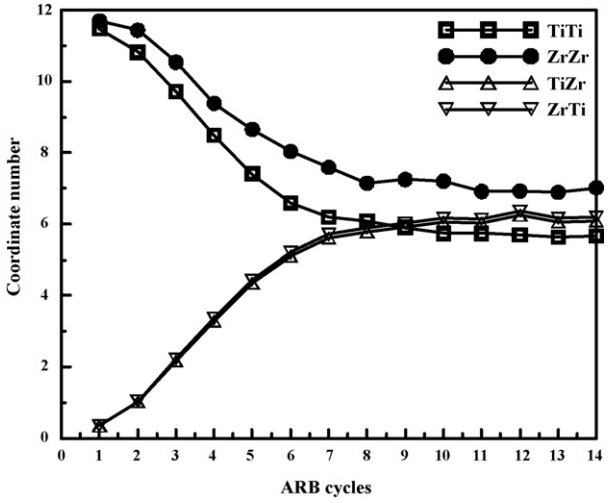

Fig. 4. The variation of average coordination number of the Zr–Ti alloys subjected to different ARB cycles.

Fig. 3 presents the partial radial distribution function (PRDF) after the ARB cycles indicated for the Zr–Ti system. Both Zr and Ti atoms need three cycles to render the peaks of crystalline become smooth. Fig. 4 presents the variation of average coordination number (CN) for every cycle. The profile of the Zr–Ti pair is referred to the case that Ti is the referenced atom and Zr is the first neighbor atom surrounding Ti. The coordination numbers of all pairs in Fig. 4 show a continuously decreasing or increasing trend until around the 6th cycle. The drop in overall system energy is not apparent in the Zr–Ti alloy system, as compared with the previous Zr–Ni simulation [20], since the mixing enthalpy of Zr–Ti is intrinsically low.

The more detailed local pairing variations with increasing ARB cycles for the Zr–Ti alloys with an ARB rolling speed of 0.025 nm fs^{-1} are depicted in Fig. 5. The pairing variation of Zr–Ti shows basically smooth and steady evolution during the ARB cycles. The close-packed initial structures characterized by the 1421 or 1422 pairs continue to decrease from 50% to less than 10% in Fig. 5(a). The overall percentage adding both 1421 and 1422 is about 20%. In contrast, the icosahedra and icosahedra-defect 1431, 1541 and 1551 pairs, characteristic of the amorphous phase continue to increase from initial 0% to an overall 60% in Fig. 5(b) for the Zr–Ti system. As shown in Fig. 5(c), the BCC-related 1441 and 1661 pairs consistently occupy minimum amounts; while the icosahedra-accompanied 1321 pairs smoothly increase to 20%. The evolution sequence as a function of ARB cycles exhibits a simple trend. There seems no intermediate atomic pairing formed during the transformation from the HCP to icosahedra (i.e., the quasi-amorphous) structure, unlike the Zr–Ni system where a BCC-like intermediate pairing was seen [20].

The current results suggest that even with the isomorphous Zr–Ti phase diagram nature, this binary system can still be vitrified through the solid-state ARB processing at room temperature, consistent with the experimental findings [17–19]. The solid-state roll bonding can offer another alternative for systems such as isomorphous Zr–Ti to form amorphous alloys, which can transform the HCP crystalline phase into complete amorphous state in a smooth sequence. During the course of atomic structure transformation, the initial fully ordered atomic close packing (100% of 1421 or 1422 pairings) can be destroyed to occupy only 20% of the overall atomic pairings. Concurrently, the much more random icosahedra and icosahedra-defect 1431, 1541 and 1551 pairs for the amorphous structure gradually become the dominant fraction of ~60%.

Since the Zr and Ti are highly similar elements with the same crystal structure, similar atomic size, hardness and melting point,

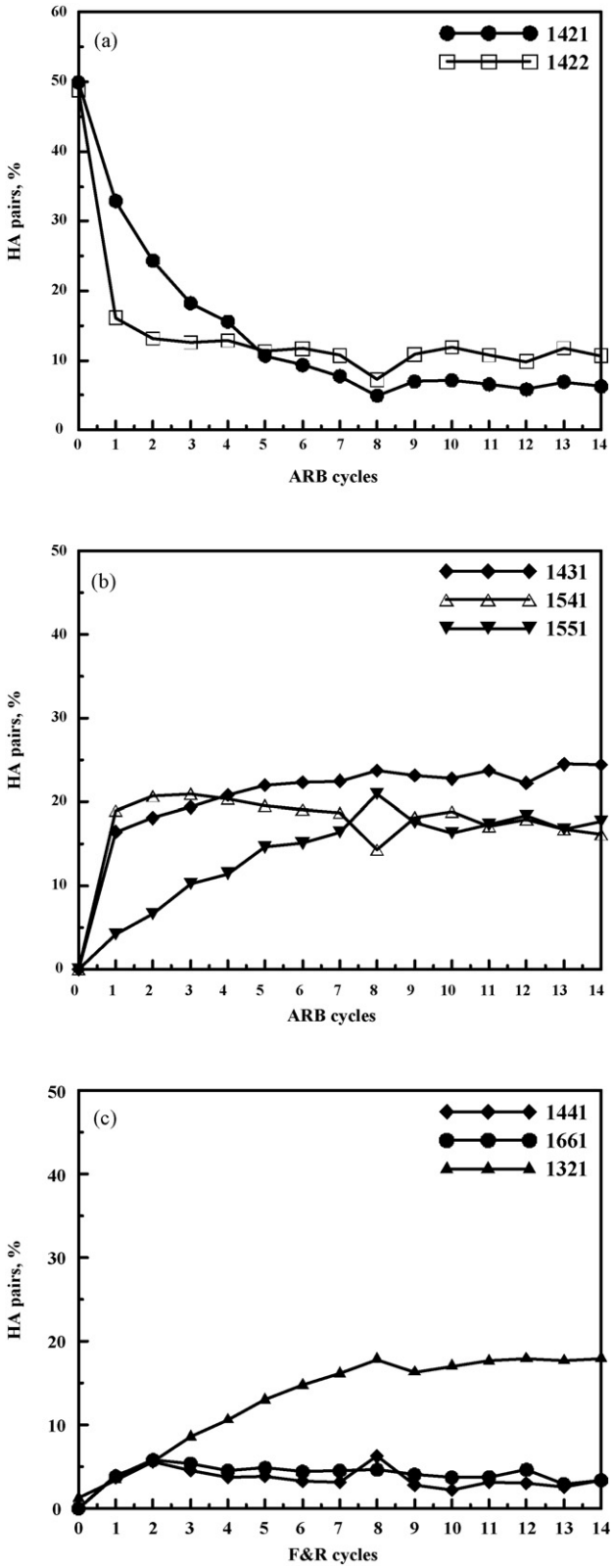

Fig. 5. The variations of the HA indices of the Zr–Ti alloys during different ARB cycles: (a) 1421 and 1422, (b) 1431, 1541, and 1551, and (c) 1441, 1661, and 1321.

and both locate on the same IVB column in the Periodical Table, they actually act as twins in many ways. Following the above scheme, it is interesting to ask whether the pure Zr (or Ti) element itself can be vitrified by itself during the same ARB route at room or cryogenic temperatures. There have been a few attempts, e.g. Refs. [35,36] to transform the crystalline pure element into the amorphous state, using torsion or ball milling, though the results are still controversial. In this study, the trial using ARB experiments on the pure Zr multilayers still could not achieve the amorphous phase. This was due to the fact that the applied rolling speed is too low and working temperature is still too high for the pure element to vitrify. On the other hand, when we adopt the more rapid ARB rolling speed and liquid nitrogen to cool the rolled specimens, the ribbons become too brittle to be rolled repeatedly. The experimental difficulty prevents from the vitrification of pure Zr. However, using the same MD simulation method, but replacing the Zr and Ti bi-layer to two pure Zr layers and running the rolling at two rolling speed of 0.01 and 0.025 nm fs^{-1}, the result might be stimulating for future experiments.

Fig. 6 shows the simulated RDF for the pure Zr at two rolling speeds. For the higher simulation rolling speed of 0.025 nm fs^{-1},

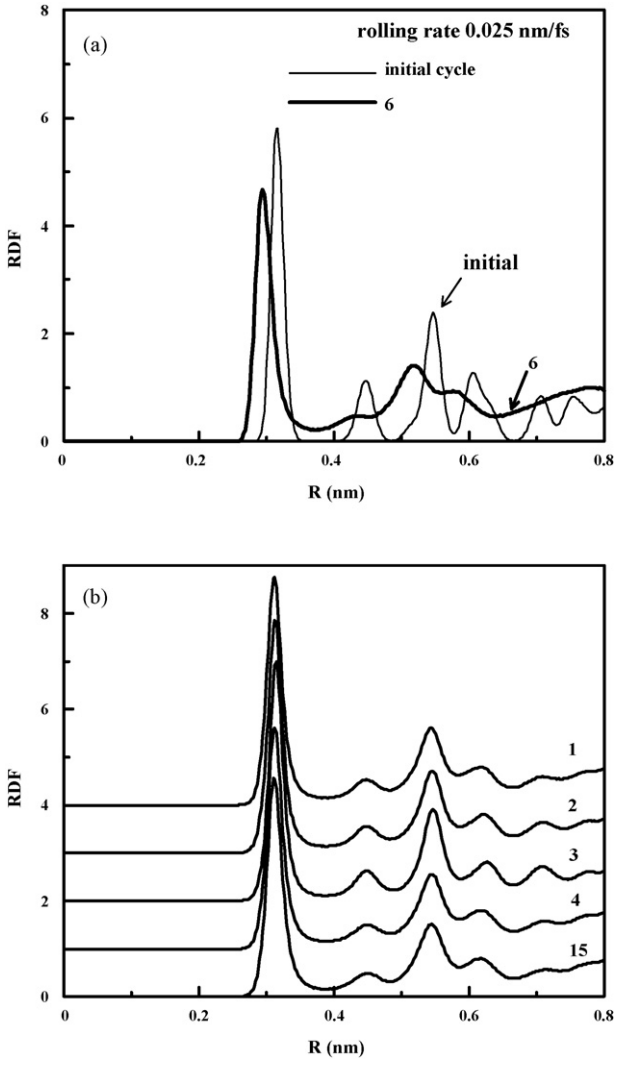

Fig. 6. The simulated RDF curves for the pure Zr bi-layers subjected to ARB with (a) a higher rolling speed of 0.025 nm fs^{-1}, and (b) a lower rolling speed of 0.01 nm fs^{-1}. The two layers of the faster case (0.025 nm fs^{-1}) become amorphous after 6 ARB cycles.

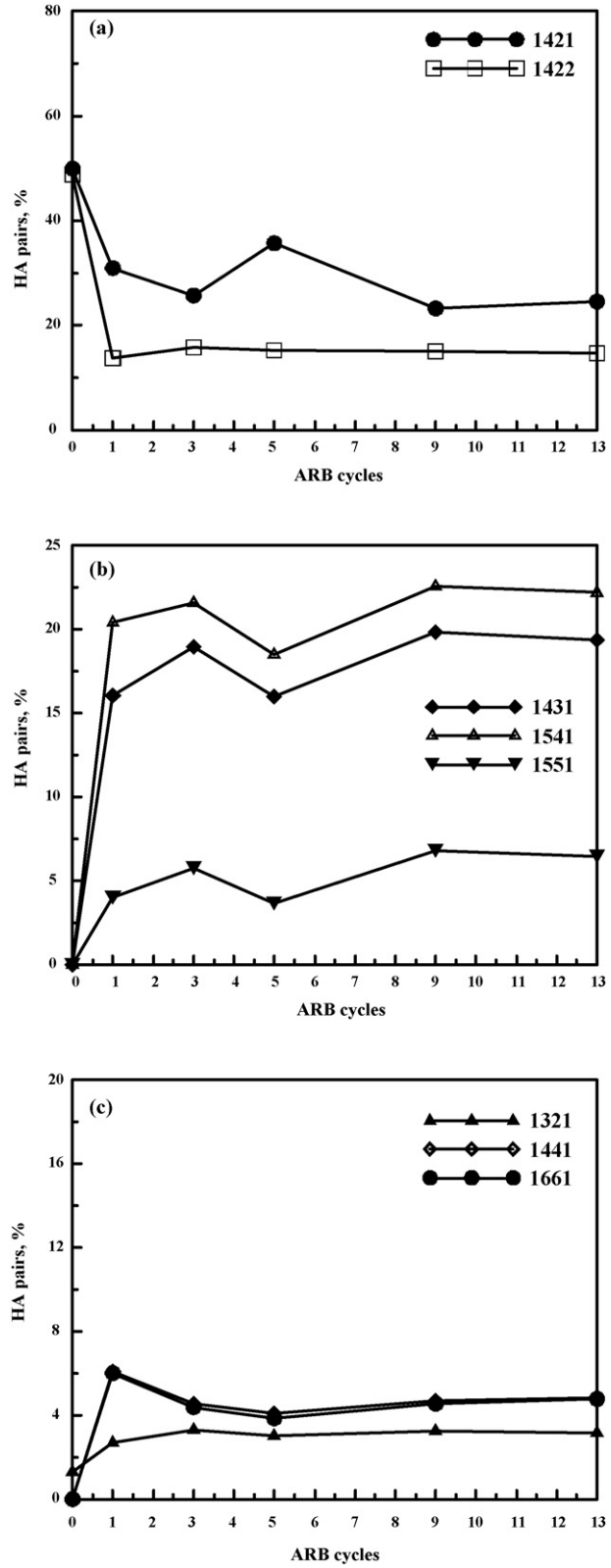

Fig. 7. The variations of the HA indices of the pure Zr during different ARB cycles at a higher speed of 0.025 nm fs^{-1}: (a) 1421 and 1422, (b) 1431, 1541, and 1551, and (c) 1441, 1661, and 1321.

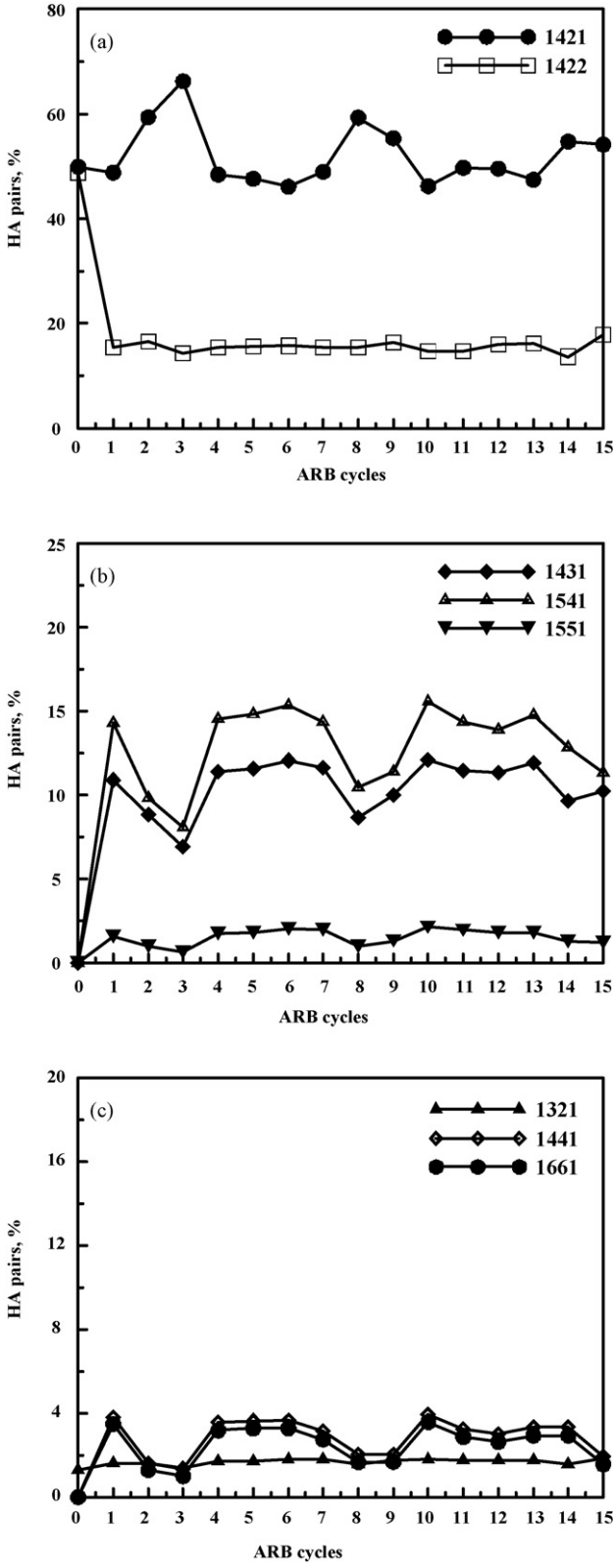

Fig. 8. The variations of the HA indices of the pure Zr during different ARB cycles at a lower speed of 0.01 nm fs^{-1}: (a) 1421 and 1422, (b) 1431, 1541, and 1551, and (c) 1441, 1661, and 1321.

and still maintaining the ambient temperature, the RDF peaks for the ordered HCP structure is seen to gradually become more and more smooth, and eventually similar to the RDF similar to amorphous materials, as depicted in Fig. 6(a). However, for the lower simulation rolling speed of 0.01 nm fs^{-1}, the HCP structure remains nearly unchanged from 1 to even 15 ARB cycles, as seen in Fig. 6(b).

The detailed atomic pairing evolution of the pure Zr during ARB at two simulation speeds are shown in Figs. 7 and 8, respectively, for the higher and lower speeds. For the case of pure Zr at the high rolling speed, as shown in Fig. 7, the HA evolution trends resemble the trends seen in the Zr–Ti binary alloy. From Fig. 7(a), it can be seen that the overall close-packed and ordered 1421 plus 1422 pairs continue to decrease from the initial 100% to overall 40% after 13 ARB cycles. At the same time, the amorphous natured icosahedra and icosahedra-defect 1431, 1541 and 1551 pairs continue to increase from the initial 0% to an overall 45% in Fig. 7(b). The rest minor 1321, 1441 and 1661 pairs consistently occupy an overall 10%. The evolution sequence as a function of ARB cycles exhibits a simple trend, similar to but not exactly the same as the Zr–Ti case. It appears that the vitrification degree of the pure Zr is consistently inferior to Zr–Ti. For example, the ordered 1421 plus 1422 pairs of Zr–Ti can be easily dropped to a minority of 20% after 10 ARB cycles, but the 1421 plus 1422 pairs of pure Zr only decrease to 40% (i.e., still a sizable portion of the persistent HCP pairing). Also, the icosahedra and icosahedra-defect 1431, 1541 and 1551 pairs, with the amorphous-like nature, can occupy ~60% in Zr–Ti, but occupy only 45% in pure Zr.

The above result for pure Zr was simulated at a faster rolling speed of 0.025 nm fs^{-1}, the situation for the pure Zr at the lower simulation rolling speed of 0.01 nm fs^{-1} reveals a different story. From the RDF curves shown in Fig. 6(b), the HCP structure is resistant to be altered. This can be confirmed from the extracted HA index, shown in Fig. 8. Now, the overall close-packed and ordered 1421 plus 1422 pairs decrease from the initial 100% to only overall 70% after 15 ARB cycles, as presented in Fig. 8(a). It means that the crystal structure of the pure Zr after 15 ARB cycles is still predominantly HCP. The amorphous-like icosahedra and icosahedra-defect 1431, 1541 and 1551 pairs together can only occupy 20%, as shown in Fig. 8(b). The rest 1321, 1441 and 1661 pairs are basically negligible. The amorphization degree is very limited in this case.

From the HA index evolution, the pure Zr seems to have the possibility to be vitrified, provided that the ARB rolling speed is sufficiently high and the working temperature is remained to be around 300 K. Experimentally, this is difficult to achieve, since the working temperature tends to rise more with increasing rolling speed. An appropriate cooling technique is necessary. Meanwhile, due to the large gap of the time scale involved in the MD simulation and real experiment, there is always room for questioning the current results (note that the rolling speed in MD is in the range of 10^{-2} nm fs^{-1} and the experimental rolling speed is around 10^{1} mm s^{-1}, or 10^{-8} nm fs^{-1}). Nevertheless, it is demonstrated by MD simulation that, under proper cooling and relative faster rolling speed, the crystalline pure Zr element could be able to transform into the amorphous phase. This is demonstrated by both the RDF curves and the HA index. Future experimental improvement is needed to justify the simulated results.

4. Summary

In summary, the local atomic pairing arrangement of the binary Zr–Ti and pure Zr systems during room temperature ARB is simulated. With the same HCP crystal structure for both Zr and Ti, the transformation in the Zr–Ti system is basically simple. No apparent transient atomic packing is formed in the intermediate stage. The icosahedra-related atomic pairs occupy nearly 80% in the later stage. The current simulation results reveal that the short-range icosahedra structures always play an important role during the course of crystalline-to-amorphous transition, both during the solid state strain-induced ARB and rapid cooling processes. Finally, it is demonstrated by MD simulation that, under proper cooling and relative faster rolling speed, the crystalline pure Zr element should be able to transform into the amorphous phase.

Acknowledgement

The authors would like to thank National Science Council of Republic of China, for supporting this study, under the grant number NSC95-2218-E-110-006.

References

[1] C.C. Koch, O.B. Cavin, C.G. Mckamey, J.O. Scarbrough, Appl. Phys. Lett. 43 (1983) 1017.
[2] J. Eckert, Mater. Sci. Eng. A226–A228 (1997) 364.
[3] N. Schultz, Mater. Sci. Eng. 97 (1998) 15.
[4] J. Lee, F. Zhou, K.H. Chung, N.J. Kim, E.J. Lavernia, Metall. Mater. Trans. A32 (2001) 3109.
[5] M. Sherif El-Eskandarany, A. Inoue, Metall. Mater. Trans. A33 (2002) 135.
[6] R.B. Schwarz, W.L. Johnson, Phys. Rev. Lett. 51 (1983) 415.
[7] X.L. Yeh, K. Samwer, W.L. Johnson, Phys. Lett. 42 (1983) 242.
[8] Y. Saito, N. Tsuji, H. Utsunomiya, T. Sakai, R.G. Hong, Scripta Mater. 39 (1998) 1221.
[9] A. Sagel, H. Sieber, H.J. Fecht, J.H. Perepzko, Acta Mater. 46 (1998) 4233.
[10] Z.P. Xing, S.B. Kang, H.W. Kim, Metall. Mater. Trans. A33 (2002) 1521.
[11] N. Tsuji, Y. Saito, S.-H. Lee, Y. Minamino, Adv. Eng. Mater. 5 (2003) 338.
[12] M. Sherif El-Eskandarany, K. Aoki, K. Sumiyama, K. Suzuki, Acta Mater. 50 (2002) 1113.
[13] M. Sherif El-Eskandarany, K. Aoki, K. Sumiyama, K. Suzuki, Scripta Mater. 36 (1997) 1001.
[14] M. Sherif El-Eskandarany, A. Inoue, Metall. Mater. Trans. A33 (2002) 2145.
[15] E. Hellstern, L. Schultz, Appl. Phys. Lett. 48 (1986) 124.
[16] J. Eckert, L. Schultz, E. Hellstern, K. Urban, J. Appl. Phys. 64 (1988) 3224.
[17] P.J. Hsieh, J.C. Huang, Y.P. Hung, S.I. Cho, J.S.C. Jang, Mater. Chem. Phys. 88 (2004) 364.
[18] P.J. Hsieh, Y.P. Hung, J.C. Huang, Scripta Mater. 49 (2003) 173.
[19] P.J. Hsieh, Y.P. Hung, S.I. Chou, J.C. Huang, Mater. Trans. JIM 45 (2004) 2686.
[20] Y.C. Lo, S.P. Ju, J.C. Huang, X.H. Du, Phys. Rev. B 76 (2007) 024103.
[21] J.D. Honeycutt, H.C. Andersen, J. Phys. Chem. 91 (1987) 4950.
[22] L. Hui, W. Guanghou, Z. Jijun, B. Xiufang, J. Chem. Phys. 116 (2002) 10809.
[23] F.F. Chen, H.F. Zhang, F.X. Qin, Z.Q. Hu, J. Chem. Phys. 120 (2004) 1826.
[24] G. Duan, D. Xu, Q. Zhang, G. Zhang, T. Cagin, W.L. Johnson, W.A. Goddard, Phys. Rev. B 71 (2005) 224208.
[25] Y.T. Zhu, X.Z. Liao, R.Z. Valiev, Appl. Phys. Lett. 86 (2005) 103112.
[26] H. Van Swygenhoven, D. Farkas, A. Caro, Phys. Rev. B 62 (2000) 831.
[27] J.F. Wax, R. Albaki, J.L. Bretonnet, Phys. Rev. B 62 (2000) 14818.
[28] T.B. Massalski, Binary Alloy Phase Diagrams, 2nd ed., ASM International, Materials Park, Ohio, USA, 1990, p. 3503.
[29] A.C. Lund, C.A. Schuh, Acta Mater. 52 (2004) 2123.
[30] F. Delogu, G. Cocco, Phys. Rev. B 71 (2005) 144108.
[31] J.M. Haile, Molecular Dynamics Simulation: Elementary Methods, John Wiley & Sons, Inc., New York, USA, 1992, p. 184.
[32] F. Cleri, V. Rosato, Phys. Rev. B 48 (1993) 22.
[33] P.J. Hsieh, Y.C. Lo, J.C. Huang, S.P. Ju, Intermetallics 14 (2006) 924.
[34] P.J. Hsieh, Y.C. Lo, C.T. Wang, J.C. Huang, S.P. Chu, Intermetallics 15 (2007) 644.
[35] J. Zhang, Y. Zhao, Nature 430 (2004) 332.
[36] T. Hattori, H. Saitoh, H. Kaneko, Y. Okajima, K. Aoki, W. Utsumi, Phys. Rev. Lett. 96 (2006) 255504.